Friction in lubricated soft-on-hard, hard-on-soft and soft-on-soft sliding contacts[☆]

Przemysław Sadowski, Stanisław Stupkiewicz[*]

Institute of Fundamental Technological Research,
Polish Academy of Sciences,
Pawińskiego 5B, 02–106 Warsaw, Poland

Abstract

Friction in lubricated soft contacts is examined using a ball-on-disc tribometer with the focus on the effect of configuration. In the soft-on-hard and hard-on-soft configurations, one of the contact-pair members is soft while the other one is hard. In the soft-on-soft configuration, both members are soft. For a soft disc, time-dependent viscoelastic deformations contribute to friction. Upon correction for the hysteretic losses, estimated using a theoretical model, the friction coefficient in the full-film regime does not depend on configuration. This holds also for high loads, when the deformations are finite. The combined effect of configuration and surface roughness on the transition from the full-film to the mixed lubrication regime is also examined.

Keywords: soft-EHL, mixed lubrication, surface roughness, finite deformation

1. Introduction

Lubricated contact of soft matter has recently become the topic of active research in engineering and biotribology. The respective engineering applications, such as elastomeric seals [1] and windscreen wipers [2], typically involve polymeric materials that are usually characterized by complex viscoelastic rheology. Even more complex material behaviour is encountered in soft tissues and biomaterials which are the members of biotribological soft contacts, such as synovial joints [3], soft artificial joints [4], eyelid wiping [5], contact lens lubrication [6], human skin contact [7], and others. The biotribological contacts may also involve non-Newtonian fluids, which introduces additional complexity and affects the tribological performance [8]. Lubricated soft contacts constitute thus one of the challenges for the modelling and simulation in tribology [9]. The soft solids themselves also attract a significant interest due to important applications, such as those in soft robotics [10] and stretchable electronics [11], as well as due to the related complex material and structural behaviour [12–14].

When the material is soft, i.e. highly compliant, a relatively small stress may cause large deformation of the solid. The related finite-deformation effects are not included in

[☆]Published in *Tribol. Int.*, vol. 129, pp. 246–256, 2019, doi: 10.1016/j.triboint.2018.08.025
[*]Corresponding author
Email addresses: psad@ippt.pan.pl (Przemysław Sadowski), sstupkie@ippt.pan.pl (Stanisław Stupkiewicz)

the classical elastohydrodynamic lubrication (EHL) theory [15, 16] which combines the Reynolds equation and the linear elasticity theory to describe, respectively, the fluid and the solid subproblem. Actually, the finite-deformation effects in soft-EHL have so far attracted only a limited interest. Finite deformations of one or both contacting members are associated with finite configuration changes, varying surface normal and area, and nonlinear material behaviour. This requires an adequate formulation of the soft-EHL problem and an adequate computational treatment [17, 18]. The lubrication surface may undergo finite deformations so that its position and shape constitute a part of the solution of the problem, and the Reynolds equation must then be formulated on a non-planar surface [18]. Moreover, it is not obvious how to formulate the Reynolds equation in non-stationary conditions when the finite deformations are time-dependent, and the lubrication surface evolves in time [19].

This work is concerned with lubricated soft contacts, and the focus is on the effect of configuration. The meaning of 'configuration' in the present context is explained below. To fix attention, let us consider a point contact in steady-state sliding, and specifically a ball sliding on a disc. This is the problem actually studied in this paper, but the considerations below apply also in more general conditions. For a ball-on-disc soft contact, one can distinguish three configurations. In the *soft-on-hard* configuration, the ball is soft and the disc is hard. In the *hard-on-soft* configuration, the ball is hard and the disc is soft. Finally, in the *soft-on-soft* configuration, both the ball and the disc are soft. Clearly, the notions of 'soft' and 'hard' are here relative. We shall assume that the difference in stiffness is high enough to treat the hard members as rigid.

In the classical EHL theory for small (infinitesimal) deformations of (perfectly) elastic bodies, there is no difference between the three configurations mentioned above. However, the configuration matters when the deformations are finite. In the soft-on-hard configuration, the contact surface remains planar, and the soft ball deforms accordingly. However, in the hard-on-soft configuration, the soft disc conforms to the rigid ball, and the contact surface is no longer planar. The contact surface is not planar in the soft-on-soft configuration either, however, the deformation pattern is different because both members undergo finite deformations.

Furthermore, when the deformations are finite, the size of the contact zone is comparable to the ball radius. Additionally, if the soft disc is relatively thin then the contact size and the surface deflections may be comparable to the disc thickness. Accordingly, the support may influence the deformations of the soft members and thus influence the lubrication conditions. Note that the classical EHL theory usually employs the elastic half-space approximation which is definitely inadequate in the conditions mentioned above.

When the soft material is viscoelastic, or characterized by a more complex rheology, then the second assumption of the classical EHL theory, i.e. the assumption of perfect elasticity, is violated. The configuration is then also an important influential factor. In the soft-on-hard configuration, the soft ball does not experience time-dependent deformations, and hence viscous effects do not really affect the steady-state contact response. However, when the disc is soft, i.e., in the hard-on-soft or soft-on-soft configuration, the disc does experience time-dependent deformations, and the viscous effects do affect the contact response. In particular, the friction force includes then the contribution related to the hysteretic losses in the disc. Additionally, at high sliding speeds, viscoelasticity may influence the deformation pattern and the shape of the contact zone, which again may influence the lubrication conditions [20].

The coefficient of rolling friction for a hard cylinder or sphere on a viscoelastic flat can be estimated using the Persson's model [21]. The model admits a general dependence of the complex modulus $E(\omega)$ on the frequency ω and thus is applicable for real viscoelastic materials with several relaxation times, as opposed to the simplified case of a single relaxation time [22, 23].

Several effects pertinent to lubricated soft contacts have already been studied experimentally. In particular, each of the three ball-on-disc configurations discussed above has been tested separately: the hard-on-soft configuration in [24–29], the soft-on-hard configuration in [30–33] and the soft-on-soft configuration in [34]. However, to the best of our knowledge, a direct comparison of the different configurations has not been performed so far.

The influence of surface roughness on the transition from the full-film hydrodynamic to the mixed lubrication regime has been studied in the hard-on-soft [24] and soft-on-soft [34] configurations. It has been shown that, for increasing surface roughness, the transition is shifted to higher values of the product of entrainment speed and lubricant viscosity ($U\eta$), while the friction coefficient in the EHL regime is not affected by surface roughness. An investigation of the effect of roughness anisotropy [26], carried out in the hard-on-soft configuration, revealed the existence of a micro-EHL regime which manifests itself in a modification of the classical shape of the Stribeck curve that exhibits then two minima of the friction coefficient. Transient elastohydrodynamic effects due to squeeze-in and squeeze-out processes in accelerated sliding have been studied in [35] showing the related quantitative effects on the Stribeck curve with respect to the steady-state sliding of rough soft contacts.

The effect of hydrophobicity has been studied in [34] in the soft-on-soft configuration. It has been shown that rendering the surfaces hydrophilic promotes the full-film lubrication regime and significantly lowers the friction coefficient in the boundary and mixed lubrication regimes. A recent study [36] of the combined effect of fluid viscosity and wetting has revealed non-conventional scaling of the Stribeck curve with lubricant viscosity due to complex multiscale interactions in rough soft contacts.

The aim of this work is to study experimentally the effect of configuration for a lubricated sliding contact with a nitrile butadiene rubber (NBR) compound used as the soft material. For that purpose, a ball-on-disc tribometer has been used in which the three configurations can be tested in the same conditions. The tribometer permits application of a relatively high load, so that moderately large deformations can be achieved. For the highest load applied in our experiments, the equivalent Hertz contact radius exceeds the fraction of 0.4–0.5 of the ball radius. This ratio is higher, in most cases significantly higher, than in the soft-EHL experiments reported in the literature, cf. [24–27, 30, 34]. Additionally, for each configuration, the effect of roughness on the transition from the full-film hydrodynamic to the mixed lubrication regime has been examined. A study of this scope has not been reported so far.

2. Experimental

2.1. Test apparatus

Friction measurements have been performed using a ball-on-disc tribometer sketched in Fig. 1. The ball is placed in a grip and loaded against a rotating flat disc. The disc is clamped to the support and both are placed in a container with a fluid. A thin layer of lubricant is continuously maintained on the disc surface to ensure lubricated

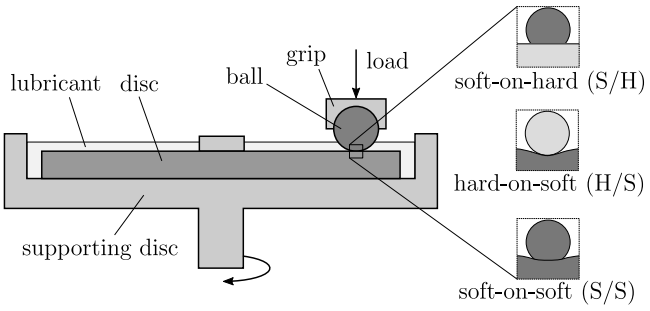

Figure 1: Ball-on-disc tribometer.

contact conditions. The normal load is applied by attaching a mass to the arm that supports the ball grip, and the friction force is measured by a load cell attached to the grip.

The ball is not allowed to rotate so that the point contact operates in a pure sliding mode, and the measurements are performed in steady-state sliding conditions. The sliding velocity v is controlled by prescribing the angular velocity of the supporting disc. The radial position of the ball that has been fixed at 42 mm. In the present experiments, the sliding speed v has been varied between 35 mm/s and 700 mm/s.

The tribometer has been designed such that three configurations can be tested for soft-EHL contacts. In the *soft-on-hard* configuration, a soft elastomeric ball is slid against a hard disc. In the *hard-on-soft* configuration, a hard ball is slid against a soft elastomeric disc. Finally, in the *soft-on-soft* configuration, both the ball and the disc are soft. The three configurations are examined in this work for a NBR rubber adopted as the soft material and steel adopted as the hard material, see the next subsection.

Another distinctive feature of the tribometer is that relatively high loads can be applied. For the maximum load of 19.3 N used in this work, and for the rubber material used, the ratio of the Hertz contact radius to the ball radius exceeds 0.4 in the case of the soft-on-hard and hard-on-soft configurations, and it exceeds 0.5 in the case of the soft-on-soft configuration. Thus the elastomeric members undergo finite deformations, and the soft-EHL contacts are tested in the finite-deformation regime.

2.2. Materials

A nitrile butadiene rubber (NBR) compound has been used to produce the soft members of the examined contact pairs. The dimensions of the rubber balls and discs are provided in Table 1. The elastic (long-term) moduls of the NBR compound has been determined equal to 1.2 MPa, based on the DMA measurements described below and further discussed in Section 3. In our previous work [18], the Young's modulus of the same compound has been estimated as 3.5 MPa by performing instrumented indentation and by fitting the resulting force–displacement response using the Hertzian theory. The two estimates are clearly different, possibly because of the difference in the deformation mode and because the viscoelastic effects might have influenced the indentation response. Throughout this work, we shall use the elastic properties resulting from the DMA measurements.

For the maximum load of 19.3 N employed in the experiments, the maximum contact pressure estimated using the Hertz theory, thus neglecting the finite-deformation

Table 1: Balls and discs used in the experimental study of soft-EHL: dimensions and root-mean-square roughness S_q.

	Dimensions [mm]	S_q [μm]
Rubber ball	$\varnothing\, 21.4$	1.30
Rubber disc	$\varnothing\, 134 \times 10$	0.70, 3.30
Steel ball	$\varnothing\, 22.2$	0.06, 2.87
Steel disc	$\varnothing\, 136 \times 2$	0.17, 1.00, 3.20

effects, is equal to 0.43 MPa for the soft-on-hard and hard-on-soft configurations and is equal to 0.28 MPa for the soft-on-soft configuration.

Thermomechanical characterization of the rubber compound has been performed using the Q800 DMA apparatus (TA Instruments). Cuboid specimens of the dimension $12.7 \times 3.3 \times 59.5$ mm have been tested in three-point bending in the sinusoidal strain-controlled mode with the displacement amplitude of 30 μm. For the chosen oscillation frequency of 0.1, 1, 10 and 100 Hz, the rubber specimen was heated up with the rate of 2°C/min from -40 to 50°C. As a result, the storage modulus E', the loss modulus E'' and the phase angle $\tan\delta = E''/E'$ have been measured as a function of the temperature. Transformation of those moduli into the frequency domain and their further usage for estimation of the friction coefficient due to hysteretic losses are described in Section 3.

Stainless steel balls and low-carbon steel discs have been used as the hard members of the examined contact pairs. Their dimensions are provided in Table 1. Steel is several orders of magnitude stiffer than the rubber compound used in the experiment, and thus it is here assumed to be rigid.

Surface roughness has been measured using a scanning profilometer (Hommel-Etamic T8000 Nanoscan). Roughness of the rubber balls and discs has been determined indirectly by measuring the roughness of the moulds that were used for producing the parts, as, e.g., in [26]. Direct measurements of the roughness of the rubber specimens have not been attempted because the rubber is too soft to perform reliable stylus profilometry measurements.

The root-mean-square roughness S_q of the untreated steel balls and discs was 0.06 μm and 0.17 μm, respectively. Steel balls and discs with a higher roughness have been produced by sandblasting. In the case of the untreated rubber balls and discs, S_q was equal to 1.30 μm and 0.70 μm, respectively. Additionally, rubber discs of a higher roughness have been produced in sandblasted moulds.

Distilled water and six silicone oils (Polsil OM oils produced by Silikony Polskie, Poland) have been used as the lubricants. Polsil OM fluids are linear, non-reactive and unmodified polydimethylsiloxanes. Different degree of polymerization results in differences of their viscosity. By selecting the adequate lubricant and by varying the angular velocity of the supporting disc, the parameter $U\eta$ could be continuously varied through a large range of values spanning more than four decades. Parameter $U\eta$, i.e., the product of the entrainment speed $U = v/2$ and lubricant viscosity η, is the main parameter specifying the hydrodynamic lubrication conditions.

The dynamic viscosity η has been measured using the Brookfield HADV-III Ultra viscometer in the cone-plate configuration at different temperatures. The results are provided in Table 2.

Table 2: Dynamic viscosity of the lubricants. The individual markers assigned to each fluid are used later on for visualisation of the experimental data.

Fluid	Marker	Dynamic viscosity η [Pa s]			
		20°C	25°C	30°C	35°C
Distilled water	□	0.001005	0.000891	0.000802	0.00072
OM 10	△	0.01045	0.00942	0.0085	0.00772
OM 50	□	0.0546	0.04895	0.04393	0.0397
OM 100	○	0.10873	0.09693	0.08727	0.0785
OM 300	◇	0.3706	0.33375	0.2982	0.2687
OM 1000	▽	1.112	0.9941	0.8868	0.7995
OM 3000	⬠	3.070	2.735	2.457	2.195

The wettability of the rubber and steel surfaces has also been measured in order to check whether the surfaces are hydrophobic or hydrophilic with respect to the lubricants used. The contact angle of a distilled water drop was found to be 79° and 89° for the steel and NBR rubber surfaces, respectively, in both cases in the test conditions achieved according to the test protocol described in Section 2.3. In the case of the silicone oils, the contact angle for each individual oil has been found to be very similar for the steel and NBR rubber surfaces. At the same time, the contact angle has been found to increase with increasing viscosity of the respective oil. Specifically, for the OM 50 oil, the contact angle was equal to 19.1° for the steel and 17.3° for the rubber, while for the OM 3000 oil it was equal to 64.4° for the steel and 63.0° for the rubber. In the case of the silicone oils, both the NBR rubber and the steel are thus hydrophilic with the degree of hydrophilicity decreasing with increasing oil viscosity. Distilled water does not follow this trend as both surfaces are then less hydrophilic than in the case of the oil of the highest viscosity. However, the Stribeck curves discussed later are consistent and do not show significant discrepancies when subsequent lubricants are used. Additionally, a visual inspection of the working surfaces after the friction measurements did not reveal the existence of wear traces. This suggests that the amount of the fluid entrained into the contact region and the good wetting properties of the fluids were sufficient to provide proper lubrication during the relatively short period of sliding contact in the mixed lubrication regime.

2.3. Test protocol

The three configurations sketched in Fig. 1 have been examined, each in a few variants of different surface roughness. Altogether, nine contact pairs have thus been tested: three soft-on-hard pairs (S/H, S/H_1, S/H_2), four hard-on-soft pairs (H/S, H/S_1, H_1/S, H_1/S_1), and two soft-on-soft pairs (S/S, S/S_1). Each contact pair has been tested under the load W equal to 0.25, 0.98, 5.13 and 19.3 N.

The nine contact pairs are listed in Table 3 along with the root-mean-square roughness S_q of the individual members and the composite roughness S_{comp} of the contact pair. In the adopted naming convention, the first character specifies whether the ball is soft ('S') or hard ('H') and similarly the second character describes the disc. The subscripts indicate that the surface roughness of the member (ball or disc) is higher than in the case of the reference member of the smallest roughness. Thus 'S/H' denotes the soft-on-hard configuration with untreated rubber ball and untreated steel

Table 3: Root-mean-square roughness (S_q, in μm) of the members of all the contact pairs tested and the corresponding composite roughness $S_{comp} = \sqrt{S_{q,B}^2 + S_{q,D}^2}$.

Roughness	S/H	S/H$_1$	S/H$_2$	H/S	H/S$_1$	H$_1$/S	H$_1$/S$_1$	S/S	S/S$_1$
ball, $S_{q,B}$	1.30	1.30	1.30	0.06	0.06	2.87	2.87	1.30	1.30
disc, $S_{q,D}$	0.17	1.00	3.20	0.70	3.30	0.70	3.30	0.70	3.30
composite, S_{comp}	1.31	1.64	3.45	0.70	3.30	2.95	4.37	1.48	3.55

disc, while 'S/H$_1$' and 'S/H$_2$' denote the contact pairs of increasing roughness of the steel disc.

For each contact pair and for a selected lubricant, the test protocol was the following. First, the ball and the disc were cleaned using ethanol for a rubber member and acetone for a steel member. The disc was clamped to the supporting disc, the ball was placed in the grip and the lubricant was poured into the container. Next, the lowest load was applied and the friction force was measured in the whole range of the sliding speed at series, starting from the lowest one. After each series of measurements with increasing sliding speed, we performed one additional measurement for the lowest speed. The results were repeatable within the usual experimental scatter. Measurements of friction as a function of the sliding speed were then repeated for subsequent increased loads.

All the steps described above were repeated for each selected lubricant. The type and number of the lubricants tested were determined for each contact pair and load in a way to catch the transition from the full-film elastohydrodynamic to the mixed lubrication regime.

3. Estimation of the hysteretic friction coefficient

In the hard-on-soft and soft-on-soft configurations, the contact zone is moving with respect to the rubber disc. The disc is thus repeatedly deformed, and this is associated with hysteretic losses in the viscoelastic rubber material. Accordingly, the measured friction force comprises then two components: the interfacial friction force and the hysteretic friction force. The interfacial friction force results from the local shear forces at the contact interface, either in the full-film hydrodynamic or in the mixed lubrication regime, and constitutes the main focus of this work. From this point of view, the hysteretic friction component is an undesired artifact. Accordingly, in this section, we estimate the hysteretic friction coefficient characteristic for the hard-on-soft and soft-on-soft configurations so that the interfacial friction can be isolated for the subsequent study. In the soft-on-hard configuration, there is no hysteretic friction because the rubber ball, once loaded by a constant load, does not deform any more. In all configurations, the hysteretic losses at the asperity scale contribute to the interfacial friction.

The overall friction coefficient μ_{tot} is assumed to be the sum of the interfacial, μ_{int} and hysteretic, μ_{hyst} parts, namely

$$\mu_{tot} = \mu_{int} + \mu_{hyst}. \tag{1}$$

The hysteretic friction coefficient μ_{hyst} is here estimated using the Persson's model of

rolling friction [21], see also [37]. The model is applicable also in the sliding mode under the assumption that the interfacial friction is low and that the fluid film separating the solids is thin, both assumptions being reasonable in the present case of lubricated contact. The model is formulated in the small-strain framework, hence the finite-deformation effects are not accounted for. The effect of thermal heating due to energy dissipation resulting from cyclic viscoelastic deformation is not accounted for either, which is here justified in view of the relatively low sliding speeds employed [38].

According to the Persson's model [21], the friction coefficient for a rigid ball rolling on a viscoelastic half-space is given by the following formula,

$$\mu_{\mathrm{hyst}} = \frac{9W}{2\pi^2} \int_0^\infty \mathrm{d}q\, q \int_0^{2\pi} \mathrm{d}\phi\, \mathrm{Im}\left(\frac{1}{E_{\mathrm{eff}}(\omega)}\right) \frac{\cos\phi}{(qa_{\mathrm{H}})^6} \left(\sin\left(qa_{\mathrm{H}}\right) - qa_{\mathrm{H}}\cos\left(qa_{\mathrm{H}}\right)\right)^2, \quad (2)$$

where

$$\omega = qv\cos\phi, \quad (3)$$

and

$$a_{\mathrm{H}} = \left(\frac{3WR}{4|E_{\mathrm{eff}}(\omega)|}\right)^{1/3}. \quad (4)$$

The friction coefficient depends on the load W, ball radius R, rolling (sliding) velocity v and complex viscoelastic modulus $E(\omega) = E'(\omega) + iE''(\omega)$, where $E'(\omega)$ and $E''(\omega)$ are the frequency-dependent storage and loss moduli, respectively. Further, $E_{\mathrm{eff}}(\omega) = E(\omega)/(1-\nu^2) = 4/3E(\omega)$ is the effective contact modulus for an incompressible material ($\nu = 0.5$), and a_{H} is the Hertz contact radius corresponding to the effective modulus $|E_{\mathrm{eff}}(\omega)|$.

The model is directly applicable to the hard-on-soft configuration. In the case of the soft-on-soft configuration, we have introduced a small modification into the model in order to account for the elastic deformation of the rubber ball. Specifically, the Hertz radius a_{H} in Eq. (4) has been evaluated using a reduced modulus $E^*_{\mathrm{eff}}(\omega)$,

$$\frac{1}{E^*_{\mathrm{eff}}(\omega)} = \frac{1-\nu^2}{E'(\omega) + iE''(\omega)} + \frac{1-\nu^2}{E'(\omega)}, \quad (5)$$

where only the real part is included in the second term in Eq. (5) because there are no hysteretic losses in the ball in pure sliding. In this way, we approximately account for the elastic deflections of the ball in the manner typical for the Hertz contact theory.

In order to characterize the viscoelastic properties of the NBR compound used in the experiment, the storage modulus E' and the loss modulus E'' have been measured using the DMA technique as a function of temperature at four excitation frequencies. The moduli have been transformed to the frequency domain by applying the time–temperature superposition principle, and the experimental master curves corresponding to the reference temperature $T = 20°\mathrm{C}$ have been determined for E' and E''. The master curves have been next fitted using the Prony series,

$$E'(\omega) = E_\infty + \sum_{k=1}^{N} E_k \frac{(\omega\tau_k)^2}{1+(\omega\tau_k)^2}, \qquad E''(\omega) = \sum_{k=1}^{N} E_k \frac{\omega\tau_k}{1+(\omega\tau_k)^2}, \quad (6)$$

where E_∞ is the long-term modulus, and E_k is the Prony coefficient corresponding to

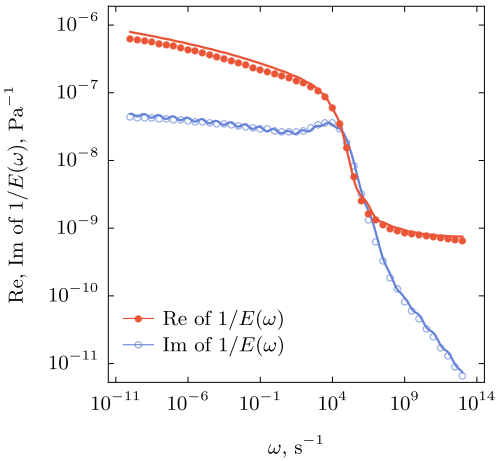

Figure 2: Real and imaginary part of the complex function $1/E(\omega)$ for the reference temperature $T = 20°\mathrm{C}$. The transformed DMA measurements (markers) have been fitted by the Prony series (solid lines).

the relaxation time τ_k.

The number of terms in the Prony series has been determined by trial and error, and $N = 24$ relaxation times τ_k have been selected in the range between 10^{-13} s and 10^{10} s, with $\tau_{k+1} = 10\tau_k$. The moduli E_∞ and E_k have been determined by fitting the inverse of the experimental complex modulus by the complex function $1/E(\omega)$, cf. [37]. The `NMinimize[]` function of *Mathematica* (www.wolfram.com) has been used for that purpose. Figure 2 shows the real and imaginary part of the complex function $1/E(\omega)$. The Prony series fit (solid lines) is compared to the transformed DMA measurements (markers). The long-term modulus has been found equal to $E_\infty = 1.2\,\mathrm{MPa}$, and this value is adopted in this work as the elastic modulus of the rubber, whenever needed.

The Persson's model can now be applied to predict the hysteretic friction in the conditions characteristic for our soft-EHL experiments. Figure 3 shows the hysteretic friction coefficient μ_{hyst} as a function of the sliding velocity v for the hard-on-soft and soft-on-soft configurations and for the four values of the load W used in the experiment. For a fixed load, the hysteretic friction coefficient is the highest at relatively high sliding velocities with the maximum at the velocity between 10 and 100 m/s, depending on the load. At the limits of $v \to 0$ and $v \to \infty$, the hysteretic losses vanish and thus $\mu_{\mathrm{hyst}} \to 0$.

The range of sliding speeds employed in the present experiment is shaded in Fig. 3. It follows that the experiments are carried out at relatively low sliding velocities, well below the range of the highest hysteretic friction. In this range, the hysteretic friction coefficient increases with increasing sliding velocity.

In whole range of sliding velocities, the hysteretic friction coefficient increases with increasing load. This is additionally illustrated in Fig. 4 which shows μ_{hyst} as a function of the load W for two sliding velocities that bound the range of the sliding velocities used in the experiment.

Finally, in the whole range of sliding velocities and normal loads, the hysteretic friction coefficient is lower in the soft-on-soft configuration than in the hard-on-soft configuration. In the conditions relevant to our experiment, the difference is significant

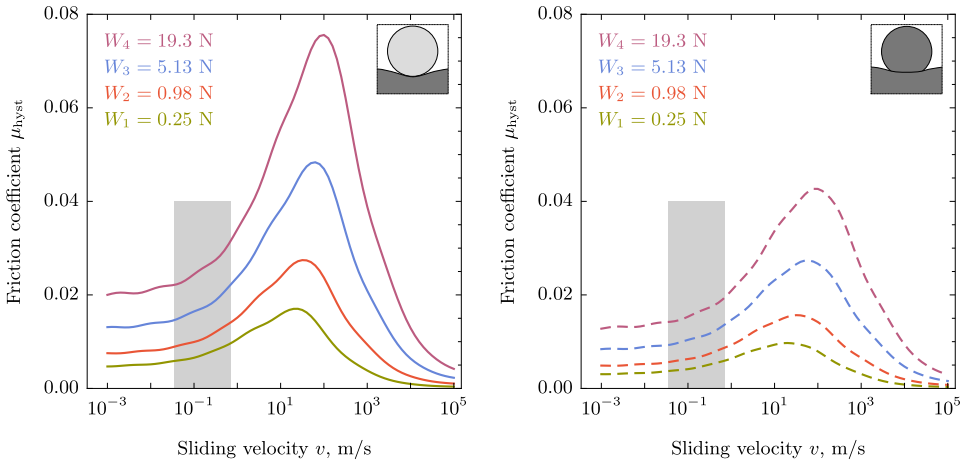

Figure 3: Hysteretic friction coefficient μ_{hyst} as a function of the sliding velocity v and load W for the hard-on-soft (a) and soft-on-soft (b) configuration. The shaded area indicates the range of sliding velocities used in experiment.

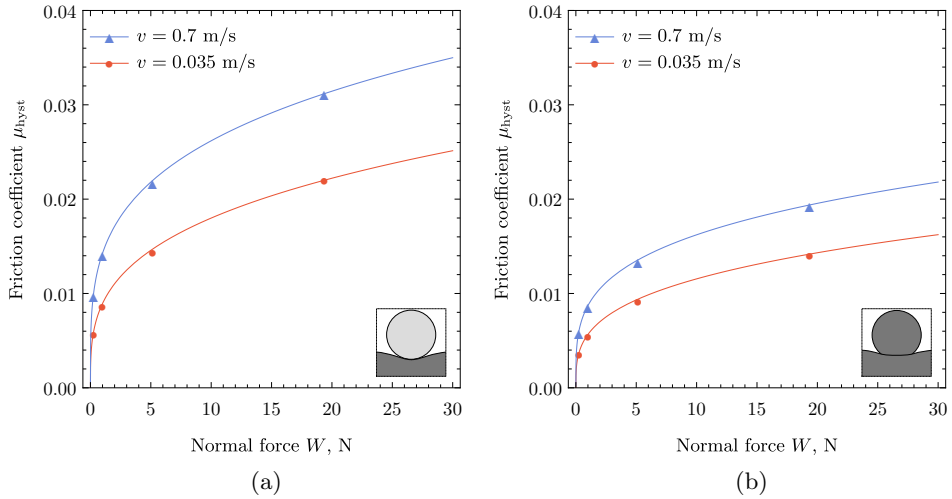

Figure 4: Hysteretic friction coefficient μ_{hyst} as a function of the load W at fixed sliding velocity for the hard-on-soft (a) and soft-on-soft (b) configuration. The individual curves correspond to two values of the sliding velocity v that bound the range of the sliding velocities used in the experiment. The markers indicate the actual loads used in experiment.

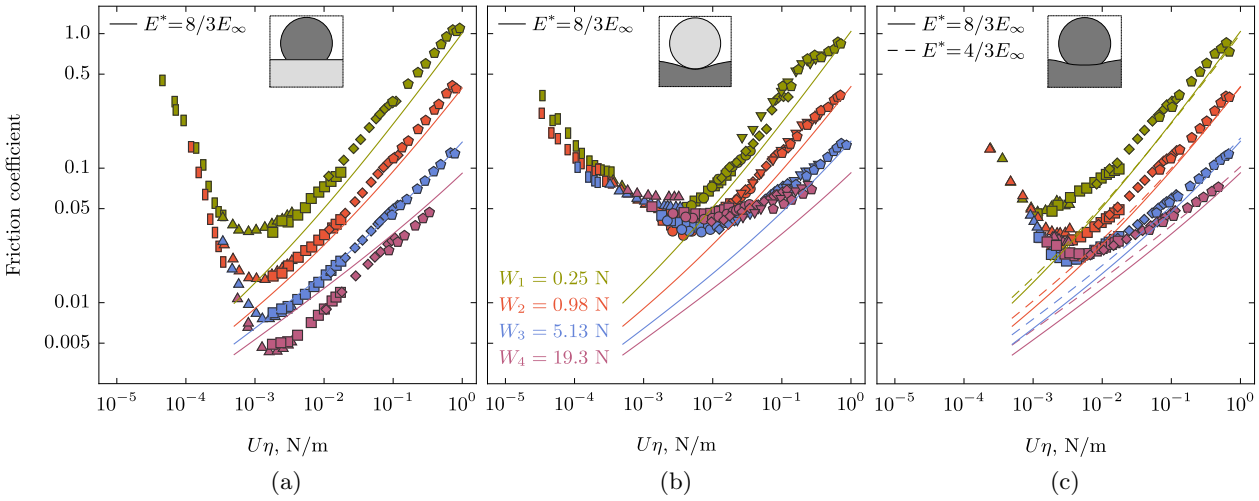

Figure 5: Friction coefficient (raw experimental data) as a function of $U\eta$ and load W for (a) soft-on-hard, (b) hard-on-soft and (c) soft-on-soft configuration. The solid lines depict the predictions of the regression equation (A.1) of de Vicente et al. [24] for the reduced modulus $E^* = 8/3E_\infty$. The dashed lines in figure (c) correspond to the reduced modulus $E^* = 4/3E_\infty$ adequate for two elastic bodies.

(30–40%), cf. Fig. 4.

4. Results and discussion

4.1. Stribeck curves: raw experimental data

Figure 5 shows the experimental Stribeck curves obtained for the three configurations studied in this work, in each case for four values of the load W. For each configuration, the results corresponding to the contact-pair members with the smallest roughness are shown (S/H, H/S and S/S pairs, cf. Table 3). The effect of surface roughness will be discussed later.

Each individual Stribeck curve represents the dependence of the friction coefficient on $U\eta$, the product of the entrainment speed U and lubricant viscosity η, which is the main parameter governing the hydrodynamic lubrication conditions. Here, the viscosity corresponding to the ambient temperature of 23 °C has been used, as the thermal effects are assumed negligible for the relatively low sliding speeds employed in the experiments.

In the full-film hydrodynamic lubrication regime, i.e. in the range of higher values of $U\eta$, the dependence of the friction coefficient on $U\eta$ is approximately linear on the log-log scale, as employed in Fig. 5. As $U\eta$ decreases from the high values, the friction coefficient decreased until a minimum is reached, which corresponds to the transition from the full-film to the mixed lubrication regime. Further decrease of $U\eta$ is associated with an increase of the friction coefficient. This is characteristic for the mixed lubrication regime in which the load is partially carried by direct asperity contacts. The fraction of direct contacts increases with decreasing $U\eta$ so that the friction coefficient increases.

In the full-film hydrodynamic lubrication regime, the friction coefficient decreases with increasing load W. In the mixed lubrication regime, the dependence on the load is much weaker.

The solid and dashed lines in Fig. 5 depict the theoretical predictions of the classical EHL theory. The regression equation (A.1) developed by de Vicente et al. [24] has been used for that purpose, see Appendix A. The underlying classical EHL theory employs the linear (small-strain) elasticity theory to model the elastic deflections of the contacting bodies. At the same time, the loads used in the present experiment are relatively high, which implies that the rubber members do experience finite deformations. Nevertheless, it follows from Fig. 5 that the predictions of the regression equation (A.1) in most cases agree reasonably well with the experimentally determined friction coefficient (of course, this only concerns the full-film EHL regime). This observation is also consistent with the results of a recent computational study of finite-deformation effects in soft-EHL [18]. Using a fully-coupled nonlinear finite-element model, it has been shown that the influence of finite deformations on the friction coefficient is insignificant for the soft-on-hard EHL point contact, even if some details of the solution of the soft-EHL problem, notably the pressure and film thickness distributions, are visibly influenced.

In the case of the hard-on-soft and soft-on-soft configurations, the experimental results corresponding to higher loads do not follow the theoretical predictions. As shown in Section 4.2, this is due to the hysteretic losses that contribute to the total friction coefficient, and the agreement is much better when the results are corrected for the hysteretic losses.

The solid lines in Fig. 5 correspond to the soft-on-hard and hard-on-soft configurations, in which one surface is rigid, and the reduced modulus E^* in the regression equation (A.1) is thus equal to $E^* = 8/3E_\infty$, see Appendix A, where E_∞ has been adopted as the Young's modulus of the rubber compound. In the case of the soft-on-soft configuration, both contacting bodies deform elastically (viscoelastic effects are not considered in the EHL theory used), and the reduced modulus E^* is redefined accordingly, $E^* = 4/3E_\infty$, see Appendix A, and the corresponding predictions of the regression equation are depicted by dashed lines in Fig. 5c. The related effects are here not significant, being more pronounced at higher loads and at lower values of $U\eta$.

4.2. Correction for the hysteretic losses

As discussed in Section 3, in the case of the hard-on-soft and soft-on-soft configurations, the measured (total) friction coefficient includes the hysteretic friction contribution. The corresponding friction coefficient μ_{hyst} has been estimated in Section 3 so that the measured friction coefficient can now be corrected for the hysteretic friction losses. This is illustrated in Fig. 6 which shows the raw experimental data, i.e. the total friction coefficient μ_{tot}, and the interfacial friction coefficient $\mu_{\mathrm{int}} = \mu_{\mathrm{tot}} - \mu_{\mathrm{hyst}}$ for the hard-on-soft configuration (H/S pair) and for the soft-on-soft configuration (S/S pair), both for the load $W_3 = 5.13\,\mathrm{N}$.

As a reference, the corresponding results for the soft-on-hard configuration (S/H pair) are also included in Fig. 6. It can be seen that, upon correction for the hysteretic losses, the friction coefficient in the elastohydrodynamic regime does not depend on the configuration, cf. the increasing branch corresponding to higher values of $U\eta$. This is discussed in more detail in the next subsection.

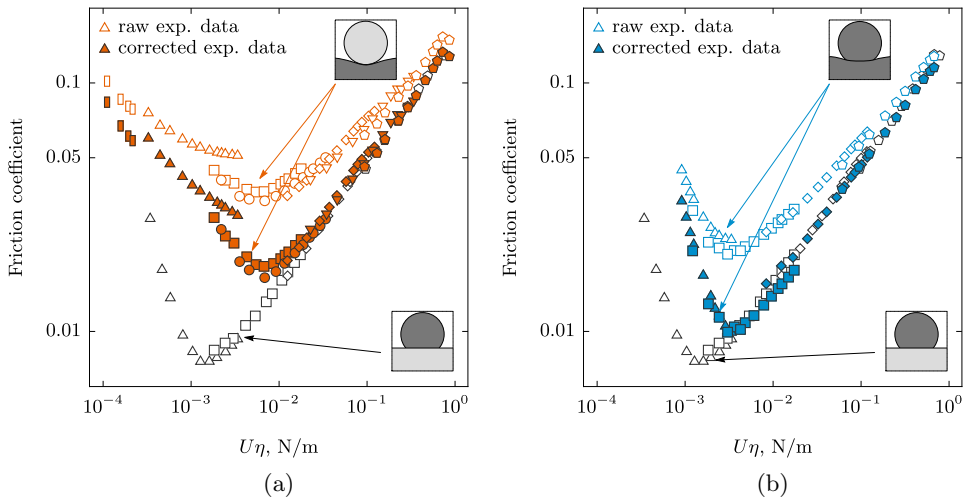

Figure 6: Friction coefficient as a function of $U\eta$: raw experimental data (empty markers) and friction coefficient corrected for hysteretic losses (filled markers) for the hard-on-soft configuration (a) and soft-on-soft configuration (b) for the load $W_3 = 5.13\,\mathrm{N}$. Results corresponding to the soft-on-hard configuration are provided as a reference.

Figure 6 illustrates yet another result of the correction for the hysteretic losses. In the experiment, there exist small ranges of the product $U\eta$ that have been examined using two lubricants of different viscosity η. Clearly, the same values of $U\eta$ have then been achieved for different entrainment speeds U. The corresponding difference in the sliding speed results in a difference in the hysteretic friction coefficient so that the total friction coefficient is typically higher for the lubricant of lower viscosity. The corresponding scatter in the measured total friction coefficient is visibly reduced by the correction for the hysteretic losses, which is apparent in Fig. 6, even if some scatter persists.

Figure 7 presents the experimental Stribeck curves that, in the case of the hard-on-soft and soft-on-soft configurations, have been corrected for the hysteretic losses. Figure 7a, which is identical to Fig. 5a, is provided here for completeness. It can be observed that, upon correction for the hysteretic losses, the full-film lubrication branches of the Stribeck curves show a visibly better agreement with the theoretical predictions (marked by solid and dashed lines) as compared to the raw experimental data in Fig. 5b,c.

Only the results corrected for the hysteretic losses are shown in the remaining part of the paper.

4.3. Effect of configuration

By examining Fig. 7, it can be concluded that, in the full-film lubrication regime, the friction coefficient does not significantly depend on the configuration. This is confirmed by Fig. 8 which compares the Stribeck curves of Fig. 7 that correspond to the same load, while the configuration is varied. Indeed, the corresponding experimental points follow a single master curve, independent of the configuration. It is recalled that, in the case of the hard-on-soft and soft-on-soft configurations, the experimental

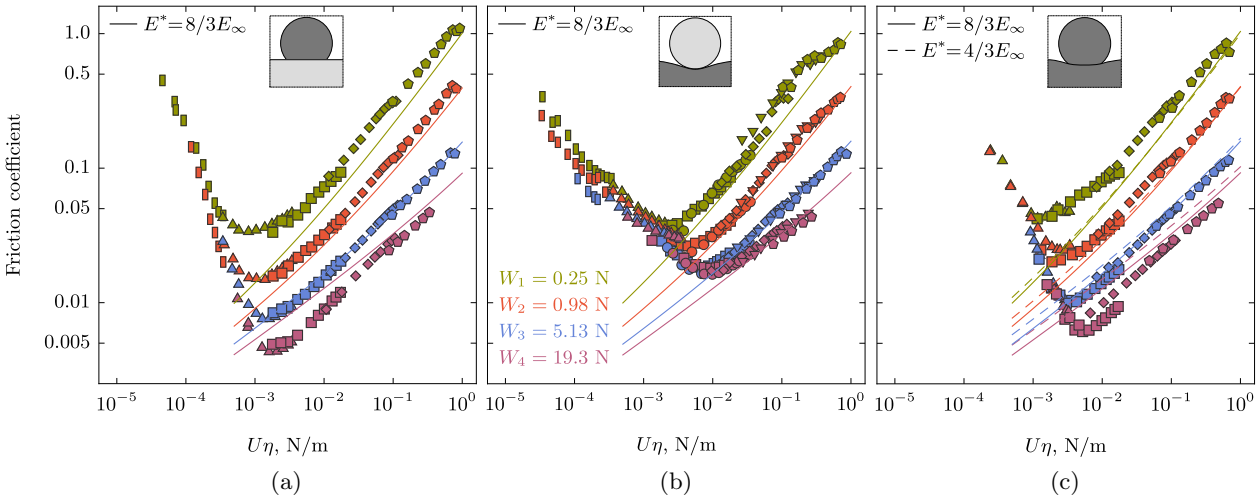

Figure 7: Friction coefficient as a function of $U\eta$ and load W for (a) soft-on-hard, (b) hard-on-soft and (c) soft-on-soft configuration. The data corresponding to the hard-on-soft and soft-on-soft configurations has been corrected for the hysteretic losses.

data has been corrected for the hysteretic losses, cf. Section 4.2. The raw data would not show such a good agreement, see Fig. 6.

While the results match perfectly in the full-film regime, the transition to the mixed lubrication regime and the slope of the mixed-lubrication branch of the Stribeck curve are visibly different in each case. Note, however, that those differences are not only related to the effect of configuration but also to the surface roughness which is different in each contact pair. The effect of roughness is examined in Section 4.4.

Figure 9 shows yet another representation of the experimental results provided in Figs. 7 and 8. Here, the friction coefficient is shown as a function of the dimensionless parameter $U\eta R/W = \bar{U}/\bar{W}$, where $\bar{U}$ and $\bar{W}$ are defined in Appendix A. It follows that, for all configurations and loads, the full-film lubrication branch of the Stribeck curve can be well approximated by a single straight line on the log-log plot. Fitting of the experimental in the full-film lubrication regime yields the following regression equation,

$$\mu_{\mathrm{EHL}} = 6.05 \left(\frac{\bar{U}}{\bar{W}} \right)^{0.547}, \qquad \frac{\bar{U}}{\bar{W}} = \frac{U\eta R}{W}, \tag{7}$$

which is shown in Fig. 9 as a solid line. The predictions of the regression equation (7) are also included in Fig. 8.

4.4. Effect of roughness

The transition from the full-film to the mixed lubrication regime is associated with the lubricant film breakdown, development of local asperity contacts and an increase of friction. As it is well known, this processes is governed by the surface roughness, see e.g. [34]. The study of the effect of configuration on friction in the full-film regime, as examined in Section 4.3, is supplemented here with a study of the influence of surface roughness on the transition from the full-film to the mixed lubrication regime.

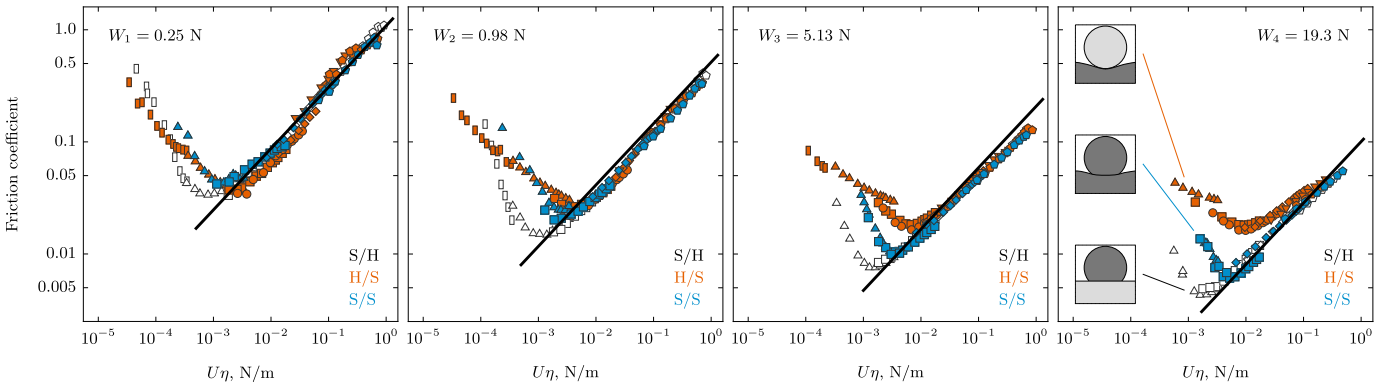

Figure 8: Effect of configuration: each figure shows the friction coefficient as a function of $U\eta$ for the three configurations at fixed load W. The solid lines show the predictions of the regression equation (7).

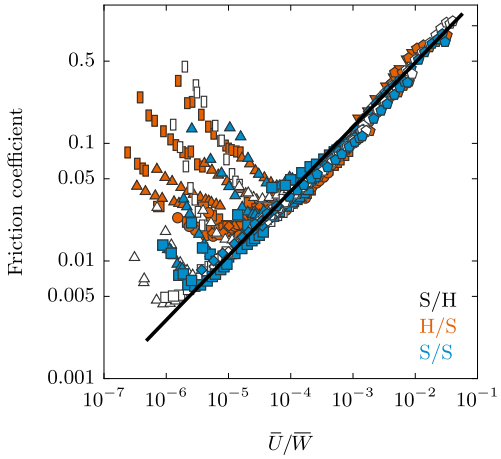

Figure 9: Effect of configuration and load: the friction coefficient is shown as a function of $\bar{U}/\bar{W}$. The solid line represents the fit by the regression equation (7).

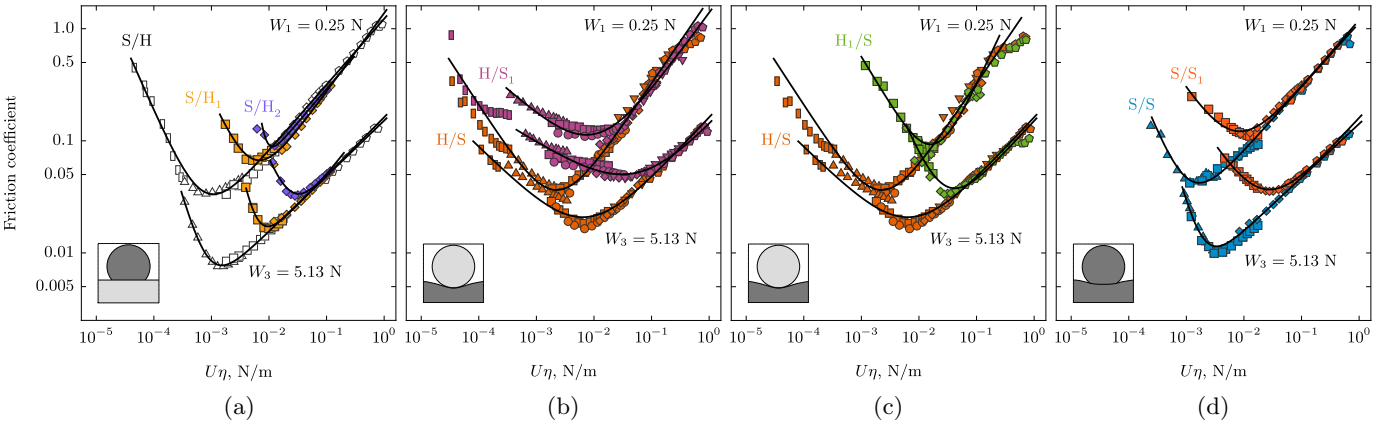

Figure 10: Effect of roughness: (a) soft-on-hard configuration, roughness of the disc is varied, (b) hard-on-soft configuration, roughness of the disc is varied, (c) hard-on-soft configuration, roughness of the ball is varied, (d) soft-on-soft configuration, roughness of the disc is varied. The solid lines represent equation (8) fitted individually to each experimental Stribeck curve.

As specified in Section 2.3, the friction measurements have been performed for nine contact pairs of different surface roughness. Selected results illustrating the effect of roughness are provided in Fig. 10 for the load $W_1 = 0.25\,\mathrm{N}$ and $W_3 = 5.13\,\mathrm{N}$. In the case of the soft-on-hard configuration, three hard discs of different roughness have been tested, and Fig. 10a shows the results obtained for the S/H$_1$ and S/H$_2$ contact pairs in addition to the reference S/H contact pair. In Fig. 10b varied is the roughness of the soft disc in the hard-on-soft configuration, and the H/S and H/S$_1$ contact pairs are shown. In Fig. 10c varied is the roughness of the hard ball in the hard-on-soft configuration, and the corresponding H/S and H$_1$/S contact pairs are shown. Finally, in Fig. 10d, the roughness of the soft disc is varied in the soft-on-soft configuration, and the S/S and S/S$_1$ contact pairs are shown. As expected, in all cases, the increase of surface roughness is associated with an increase of the value of $U\eta$ that corresponds to the transition from the full-film to the mixed lubrication regime.

In order to characterize the effect of roughness in hydrodynamic lubrication, the composite roughness of the contact pair is usually referred to the average thickness of the lubricant film, and the fraction of the latter to the former, denoted by Λ, is used for that purpose [16]. In the thick-film regime, for $\Lambda > 10$, the effect of roughness is negligible. In the thin-film regime, which corresponds to $3 < \Lambda < 10$, the surfaces are separated by the lubricant film, however, the fluid flow is affected by the roughness. Finally, in the mixed lubrication regime, for $\Lambda < 3$, direct asperity contacts occur and carry a part of the load. The above classification is a simplification of the complex reality, particularly in soft contacts in which the actual roughness may significantly differ from the initial, undeformed roughness. Furthermore, the asperity-scale phenomena in micro-lubrication may be influenced by additional factors, in particular, whether the roughness is on the soft or on the hard surface, and whether it is on the moving or on the stationary surface. Nevertheless, it is of interest to examine whether the limit value of $\Lambda = 3$, evaluated in terms of the initial composite roughness, may serve as an indicator for the transition from the full-film to the mixed lubrication regime. This is pursued below.

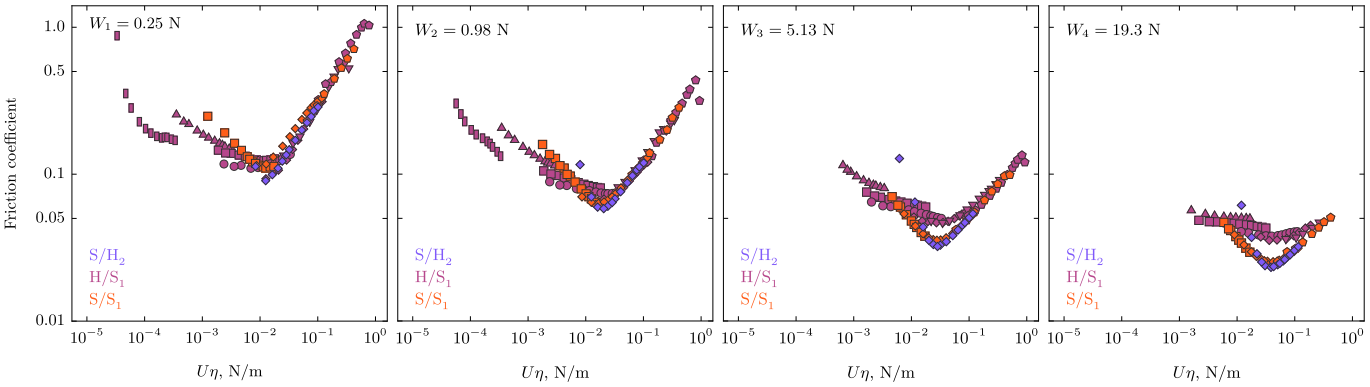

Figure 11: Friction coefficient as a function of $U\eta$ for three contact pairs (S/H$_2$, H/S$_1$ and S/S$_1$) that have a similar composite roughness S_{comp}.

Three of the tested contact pairs, specifically S/H$_2$, H/S$_1$ and S/S$_1$, each representing one of the three configurations, are characterized by a similar composite roughness, between 3.30 μm and 3.55 μm, see Table 3. Figure 11 shows the friction coefficient as a function of $U\eta$ for those three contact pairs, separately for each load. It can be seen that, at a fixed load, the minimum of the friction coefficient corresponds for each contact pair to a very similar value of $U\eta$ that depends on the load. This observation supports the assumption that the composite roughness is a relevant quantity governing the transition from the full-film to the mixed lubrication regime.

In the following we shall examine the working assumption that the minimum of the friction coefficient corresponds to the lubricant-film breakdown, and that this occurs at $\Lambda = 3$, where Λ is defined in terms of the composite roughness S_{comp} and minimum film thickness h_{m}, i.e. $\Lambda = h_{\text{m}}/S_{\text{comp}}$. In order to verify this assumption, the minimum film thickness will be calculated using the regression equation (A.2) of de Vicente et al. [24]. According to this equation, the minimum film thickness depends on $U\eta$, and here the value corresponding to the experimentally determined minimum of the friction coefficient will be used.

The value of $U\eta$ that corresponds to the minimum of the experimental friction coefficient has been determined by fitting each experimental Stribeck curve and by finding the minimum on the fitting curve. The following function has been used for that purpose,

$$\mu_{\text{int}} = \mu_{\text{EHL}} + \mu_{\text{mixed}}, \qquad \mu_{\text{EHL}} = a(U\eta)^p, \qquad \mu_{\text{mixed}} = b(U\eta)^q, \tag{8}$$

where a, b, p and q are the fitting parameters. The first term, μ_{EHL}, corresponds to the full-film lubrication regime, while the second term, μ_{mixed}, corresponds to the mixed lubrication regime. Accordingly, we have $p > 0$ and $q < 0$, and each term individually is represented on the log-log plot by a straight line of a positive (μ_{EHL}) or negative (μ_{mixed}) slope. In most cases, the simple function (8) provides a very good fit of the experimental data, as illustrated in Fig. 10. Note that the regression equation (7) could be employed in Eq. (8) instead of fitting μ_{EHL} individually for each experimental Stribeck curve. The latter approach has been adopted as it has turned to provide a better estimation of the minima on the individual Stribeck curves.

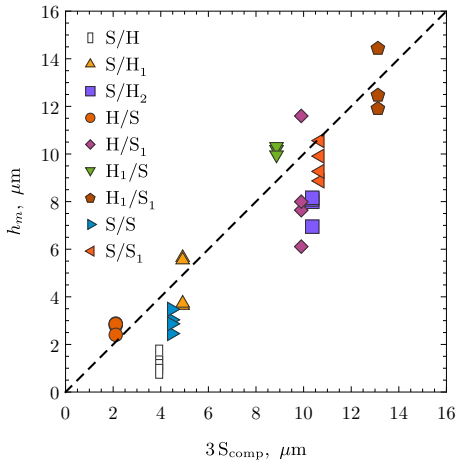

Figure 12: Dependence between the minimum film thickness h_{m} and the composite roughness S_{comp}. The minimum film thickness has been estimated using Eq. (A.2) in which $U\eta$ corresponds to the minimum of the friction coefficient for a fixed contact pair and load. The dashed line corresponds to $h_{\mathrm{m}} = 3S_{\mathrm{comp}}$, i.e. to $\Lambda = 3$.

Figure 12 shows the minimum film thickness h_{m}, determined according to the procedure described above, as a function of the composite roughness S_{comp} multiplied by the factor of three. Each data point represents h_{m} determined individually for each contact pair and for each load. The points corresponding to a fixed contact pair are arranged vertically, as they share the same composite roughness S_{comp}. The data gathered in Fig. 12 shows some scatter, however, in general the individual points follow the trend line of $h_{\mathrm{m}} = 3S_{\mathrm{comp}}$ (marked by the dashed line in Fig. 12), which supports our working assumption.

Recall that Λ has been here determined in terms of the initial surface roughness. However, particularly in soft contacts, the asperities may deform, and attenuation of surface roughness may be responsible for the deviation of the data in Fig. 12 from the trend line of $h_{\mathrm{m}} = 3S_{\mathrm{comp}}$. Other plausible reasons for this deviation include inadequacy of the assumption that the lubricant breakdown corresponds to the minimum of the friction coefficient, errors in estimating the location of the minimum of the friction coefficient, inaccuracy of the minimum film thickness equation (A.2), e.g., due to the finite-deformation effects [18], and influence of surface roughness on the average film thickness. All those effects may also contribute to the scatter of the points that correspond to a fixed contact pair.

Nevertheless, most of the data points in Fig. 12 lie below the dashed line, and the deviation towards the zone of $h_{\mathrm{m}} < 3S_{\mathrm{comp}}$ is visibly more pronounced than towards $h_{\mathrm{m}} > 3S_{\mathrm{comp}}$. This can be interpreted as the effect of attenuation of surface roughness.

The S/H pair is characterized by the smallest value of Λ at film breakdown, equal to $\Lambda = 0.9 \pm 0.3$. The S/H pair is composed of a relatively smooth hard disc ($S_{\mathrm{q}} = 0.17\,\mu$m) and significantly rougher soft ball ($S_{\mathrm{q}} = 1.30\,\mu$m). Note that the asperities on the ball surface are stationary with respect to the contact zone so that they do not experience time-dependent deformations, which makes them highly compliant. In these conditions, the surface roughness can be significantly reduced in the thin-film regime thus explaining the low value of Λ at film breakdown.

For two contact pairs, the value of Λ at film breakdown is also visibly smaller than three, namely $\Lambda = 2.0 \pm 0.3$ for the S/S pair and $\Lambda = 2.3 \pm 0.2$ for the S/H_2 pair. For the remaining contact pairs, the deviation from $\Lambda = 3$ is not much pronounced. In particular, the condition $\Lambda = 3$ is not much affected by the configuration.

5. Conclusion

The effect of configuration of soft and hard members in a lubricated sliding contact has been studied experimentally. In the hard-on-soft and soft-on-soft configurations, the measured friction force includes the contribution due to the hysteretic losses in a viscoelastic disc. The corresponding friction coefficient has thus been estimated using the Persson's model [21], and the experimental data has been corrected for the hysteretic losses. Upon this correction, the configuration is shown not to affect the resulting friction coefficient in the full-film EHL regime for all loads studied, also for high loads that induce finite deformations of the soft members.

The effect of the load and sliding speed ($U\eta$) on the friction coefficient is well described by the classical EHL theory, as represented by the regression equation of de Vicente et al. [24]. Actually, in the EHL regime, the Stribeck curves corresponding to the different loads merge into a single straight line on the log-log plot when the dimensionless speed is normalized by the dimensionless load.

The effect of surface roughness has been examined by testing the total of nine contact pairs, each characterized by a different composite roughness and representing one of the three configurations. In agreement with the previous studies, the transition from the full-film to the mixed lubrication regime has been found to be governed by surface roughness. Increasing surface roughness shifts the transition to higher values of $U\eta$, while it does not influence the friction coefficient in the EHL regime. It has been confirmed that the criterion $\Lambda = 3$, where Λ is determined in terms of the minimum film thickness and initial composite roughness, can be used in most cases as an indicator for the transition from the full-film to the mixed lubrication regime. The effect of configuration is here not much pronounced regardless whether the roughness is on the soft or hard surface and whether the roughness is stationary or moving with respect to the contact zone.

Appendix A. Regression equations of de Vicente et al. [24]

Based on the predictions of the classical EHL theory, de Vicente et al. [24] proposed regression equations for the friction coefficient and minimum film thickness in soft-EHL rolling–sliding point contacts. In the case of pure sliding, as employed in our experiments, the friction coefficient corresponding to the force acting on the ball is given by the following formula,

$$\mu_{\mathrm{reg}} = 2\left(3.8\bar{U}^{0.71}\overline{W}^{-0.76} + 0.96\bar{U}^{0.36}\overline{W}^{-0.11}\right) - 1.46\bar{U}^{0.65}\overline{W}^{-0.70}, \qquad \text{(A.1)}$$

where $\bar{U} = U\eta/(E^*R^*)$ and $\overline{W} = W/(E^*R^{*2})$. When one of the surfaces is planar, the reduced radius R^* is equal to the ball radius R, i.e. $R^* = R$. When one of the contacting bodies is rigid, i.e. for the soft-on-hard or hard-on-soft configuration, the reduced modulus E^* is equal to $8/3E$, where E is the Young's modulus of the elastic

body, and $\nu = 0.5$ is assumed in view of incompressibility. When both bodies are elastic and have equal Young's moduli, the reduced modulus E^* is equal to $4/3E$. The minimum film thickness h_{m} has been fitted by the following formula,

$$\frac{h_{\mathrm{m}}}{R^*} = 2.8\overline{U}^{0.66}\overline{W}^{-0.22}. \tag{A.2}$$

Acknowledgement

This work has been partially supported by the National Science Center (NCN) in Poland under Grant no. 2011/01/B/ST8/07434. The tribometer used in this study has been designed and constructed with the assistance of Prof. Stanisław Kucharski, IPPT, and this is gratefully acknowledged. The authors are also grateful to Emilia Choińska and Ewelina Kozikowska, Joint Laboratory of Multifunctional Materials, IPPT, for performing wettability and DMA measurements, respectively, and Piotr Denis, Laboratory of Polymers and Biomaterials, IPPT, for performing viscosity measurements.

References

[1] Müller HK, Nau BS. Fluid Sealing Technology: Principles and Applications. Marcel Dekker, Inc., New York; 1998.

[2] Fujii Y. Method for measuring transient friction coefficients for rubber wiper blades on glass surface. Tribol Int 2008;41:17–23.

[3] Ateshian GA. The role of interstitial fluid pressurization in articular cartilage lubrication. J Biomech 2009;42:1163–1176.

[4] Lu X, Meng Q, Wang J, Jin Z. Transient viscoelastic lubrication analyses of UHMWPE hip replacements. Tribol Int 2018;128:271–278.

[5] Jones MB, Fulford GR, Please CP, McElwain DLS, Collins MJ. Elastohydrodynamics of the eyelid wiper. Bull Math Biol 2008;70:323–343.

[6] Dunn AC, Tichy JA, Urueña JM, Sawyer WG. Lubrication regimes in contact lens wear during a blink. Tribol Int 2013;63:45–50.

[7] Adams MJ, Briscoe BJ, Johnson SA. Friction and lubrication of human skin. Tribol Lett 2007;26:239–253.

[8] de Vicente J, Stokes JR, Spikes HA. Soft lubrication of model hydrocolloids. Food Hydrocolloids 2006;20:483–491.

[9] Vakis AI, Yastrebov VA, Scheibert J, Nicola L, Dini D, Minfray C, et al. Modeling and simulation in tribology across scales: An overview. Tribol Int 2018;125:169–199.

[10] Rus D, Tolley MT. Design, fabrication and control of soft robots. Nature 2015;521:467–475.

[11] Lin S, Yuk H, Zhang T, Parada GA, Koo H, Yu C, et al. Stretchable hydrogel electronics and devices. Adv Mater 2016;28:4497–4505.

[12] Bertoldi K, Reis PM, Willshaw S, Mullin T. Negative Poisson's ratio behavior induced by an elastic instability. Adv Mater 2010;22:361–366.

[13] Lin S, Mao Y, Radovitzky R, Zhao X. Instabilities in confined elastic layers under tension: Fringe, fingering and cavitation. J Mech Phys Solids 2017;106:229–256.

[14] Bigoni D, Bordignon N, Piccolroaz A, Stupkiewicz S. Bifurcation of elastic solids with sliding interfaces. Proc R Soc London, Ser A 2018;474:20170681.

[15] Dowson D, Higginson GR. Elasto-hydrodynamic lubrication. Pergamon Press, Oxford; 1977.

[16] Hamrock BJ, Schmid SR, Jacobson BO. Fundamentals of Fluid Film Lubrication. Second ed.; Marcel Dekker, Inc., New York; 2004.

[17] Stupkiewicz S. Finite element treatment of soft elastohydrodynamic lubrication problems in the finite deformation regime. Comput Mech 2009;44:605–619.

[18] Stupkiewicz S, Lengiewicz J, Sadowski P, Kucharski S. Finite deformation effects in soft elastohydrodynamic lubrication problems. Tribol Int 2016;93:511–522.

[19] Temizer I, Stupkiewicz S. Formulation of the Reynolds equation on a time-dependent lubrication surface. Proc R Soc London, Ser A 2016;472:20160032.

[20] Putignano C, Dini D. Soft matter lubrication: does solid viscoelasticity matter? ACS Appl Mater Interfaces 2017;9:42287–42295.

[21] Persson BNJ. Rolling friction for hard cylinder and sphere on viscoelastic solid. Eur Phys J E 2010;33:327–333.

[22] Hunter SC. The rolling contact of a rigid cylinder with a viscoelastic half space. J Appl Mech 1961;28:611–617.

[23] Goryacheva IG. Contact Mechanics in Tribology. Kluwer, Dordrecht; 1998.

[24] de Vicente J, Stokes JR, Spikes HA. The frictional properties of Newtonian fluids in rolling–sliding soft-EHL contact. Tribol Lett 2005;20:273–286.

[25] Myant C, Spikes HA, Stokes JR. Influence of load and elastic properties on the rolling and sliding friction of lubricated compliant contacts. Tribol Int 2010;43:55–63.

[26] Scaraggi M, Carbone G, Dini D. Experimental evidence of micro-EHL lubrication in rough soft contacts. Tribol Lett 2011;43:169–174.

[27] Carbone G, Putignano C. A novel methodology to predict sliding and rolling friction of viscoelastic materials: Theory and experiments. J Mech Phys Solids 2013;61:1822–1834.

[28] Cassin G, Heinrich E, Spikes HA. The influence of surface roughness on the lubrication properties of adsorbing and non-adsorbing biopolymers. Tribol Lett 2001;11:95–102.

[29] Marx N, Guegan J, Spikes HA. Elastohydrodynamic film thickness of soft EHL contacts using optical interferometry. Tribol Int 2016;99:267–277.

[30] Persson BNJ, Scaraggi M. On the transition from boundary lubrication to hydrodynamic lubrication in soft contacts. J Phys: Condens Matter 2009;21:185002.

[31] Bongaerts JHH, Day JPR, Marriott C, Pudney PDA, Williamson AM. *In situ* confocal Raman spectroscopy of lubricants in a soft elastohydrodynamic tribological contact. J Appl Phys 2008;104:014913.

[32] Myant C, Fowell M, Cann P. The effect of transient motion on Isoviscous–EHL films in compliant, point, contacts. Tribol Int 2014;72:98–107.

[33] Putignano C, Reddyhoff T, Carbone G, Dini D. Experimental investigation of viscoelastic rolling contacts: a comparison with theory. Tribol Lett 2013;51:105–113.

[34] Bongaerts JHH, Fourtouni K, Stokes JR. Soft-tribology: Lubrication in a compliant PDMS–PDMS contact. Tribol Int 2007;40:1531–1542.

[35] Scaraggi M, Dorogin L, Angerhausen J, Murrenhoff H, Persson BNJ. Elastohydrodynamics for soft solids with surface roughness: Transient effects. Tribol Lett 2017;65:95.

[36] Selway N, Chan V, Stokes JR. Influence of fluid viscosity and wetting on multiscale viscoelastic lubrication in soft tribological contacts. Soft Matter 2017;13:1702–1715.

[37] Scaraggi M, Persson BNJ. Rolling friction: comparison of analytical theory with exact numerical results. Tribol Lett 2014;55:15–21.

[38] Putignano C, Le Rouzic J, Reddyhoff T, Carbone G, Dini D. A theoretical and experimental study of viscoelastic rolling contacts incorporating thermal effects. Proc Inst Mech Eng J 2014;228:1111–1121.